^{142}Nd Evidence for Early (>4.53 Ga) Global Differentiation of the Silicate Earth

M. Boyet* and R. W. Carlson

New high-precision samarium-neodymium isotopic data for chondritic meteorites show that their ^{142}Nd/^{144}Nd ratio is 20 parts per million lower than that of most terrestrial rocks. This difference indicates that most (70 to 95%) of Earth's mantle is compositionally similar to the incompatible element–depleted source of mid-ocean ridge basalts, possibly as a result of a global differentiation 4.53 billion years ago (Ga), within 30 million years of Earth's formation. The complementary enriched reservoir has never been sampled and is probably located at the base of the mantle. These data influence models of Earth's compositional structure and require revision of the timing of global differentiation on Earth's Moon and Mars.

Radiogenic isotope tracers are often used to understand the chemical evolution of planetary bodies. In one system, Sm decays to Nd via two radioactive decay schemes: ^{146}Sm-^{142}Nd [half-life $T_{1/2}$ = 103 million years (My)] and ^{147}Sm-^{143}Nd [$T_{1/2}$ = 106 billion years (Gy)]). Both Sm and Nd are refractory lithophile (prefer silicates over metal) elements, whose relative abundances should not be affected by either volatile loss or core formation. The long-lived ^{147}Sm-^{143}Nd system has been widely used to trace planetary-scale processes such as the evolution of the bulk silicate Earth (BSE, defined as all the Earth except for its metallic core) and its chemical differentiation into crust and mantle over Earth's history. The early epic of Earth's differentiation is better investigated with the short-lived chronometer ^{146}Sm-^{142}Nd, because of the lack of available samples from Earth's first 500 My of existence and the sensitivity of most long-lived radioactive systems to resetting by events occurring later in Earth's history. Recent studies have reported small ^{142}Nd/^{144}Nd excesses in a small number of samples from 3.8 Ga from the Isua Supracrustal Belt, Greenland (*1*, *2*), which is the first evidence for differentiation of the silicate portion of Earth that must have occurred close in time to the well-documented early differentiation of the Moon (*3*) and Mars (*4*, *5*). The standard assumption in using this radiometric system to model the geochemical evolution of Earth is that the BSE has Sm/Nd, ^{143}Nd/^{144}Nd, and ^{142}Nd/^{144}Nd ratios approximately equal to those of chondritic meteorites, the building blocks of the planet. Chondritic meteorites show a relatively limited range in Sm/Nd (^{147}Sm/^{144}Nd from 0.1932 to 0.2000), with corresponding ^{143}Nd/^{144}Nd from 0.512525 to 0.512722, when fractionation is corrected to ^{146}Nd/^{144}Nd = 0.7219 (*6*–*8*), and the average chondritic values of 0.1966 and 0.512638 (*6*) have been used to represent the BSE model values for 25 years. Here we present Sm-Nd data from chondrites that overlap previous Sm/Nd and ^{143}Nd/^{144}Nd ratio determinations but indicate a measurable difference of ^{142}Nd/^{144}Nd ratios between chondrites and all terrestrial samples. If the BSE has an Sm/Nd ratio within the range measured for chondrites, the higher-than-chondritic ^{142}Nd/^{144}Nd ratio of terrestrial materials requires that the silicate Earth experienced a global chemical differentiation during the lifetime of ^{146}Sm, resulting in high and complementary low Sm/Nd ratio reservoirs that have remained separate over all of Earth's history.

Terrestrial Sm-Nd evolution. The most active volcanic system on Earth, the global ocean ridge system, erupts magmas with ^{143}Nd/^{144}Nd ratios considerably higher than any value measured for bulk chondritic meteorites. This value reflects the high Sm/Nd ratio and the general depletion of the oceanic mantle in those elements that selectively partition into melts (the so-called incompatible elements), because Nd is more incompatible than Sm. The incompatible element depletion of the mid-ocean ridge basalt (MORB) source generally is modeled as resulting from the extraction of the incompatible element–rich continental crust over Earth's history. To explain the high Sm/Nd in the MORB source purely by continental crust extraction from a mantle that initially had chondritic Sm/Nd, only roughly one-third to one-half of the mantle can be as incompatible element–depleted as the MORB source (*9*–*11*). The rest of the mantle has typically been assumed to have remained primitive, with a chondritic Sm/Nd ratio. However, some observations are difficult to reconcile with this model (*12*, *13*). For example, recent seismic imaging of the mantle suggests that convective motion may stir at least the upper three-quarters of the mantle (*14*), if not most of it. Also, the oldest crustal rocks on Earth (dating to 4 Ga) have superchondritic ^{143}Nd/^{144}Nd ratios, requiring an episode of even earlier crustal extraction, although only volumetrically insignificant amounts of this pre–4-Ga crust survive at Earth's surface today (*15*, *16*). Other evidence that the incompatible element depletion that now characterizes the MORB source mantle is an old feature, not related to the formation of the current continental crust, is the presence of excess ^{129}Xe (derived from the decay of 17-My–half-life ^{129}I) and Pu-fission Xe in the MORB, which indicate that the source must have been outgassed within 50 My of Earth's formation (*17*, *18*).

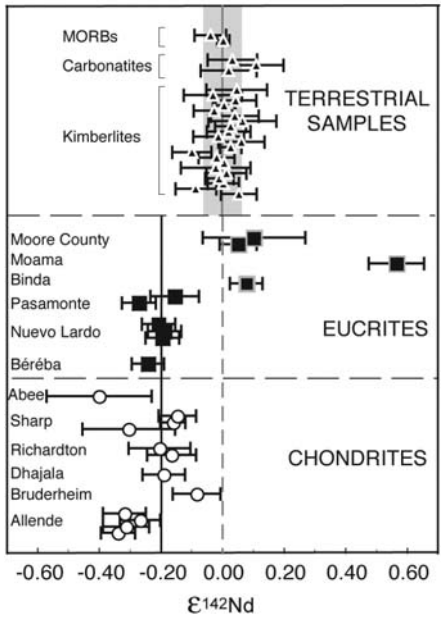

Fig. 1. ^{142}Nd/^{144}Nd ratios measured for chondrites and eucrites compared to the La Jolla terrestrial Nd standard (ε^{142}Nd). All chondrites and basaltic eucrites have negative ε^{142}Nd values outside the external analytical error of ± 0.07 ε units (2σ) (shaded area). Cumulate eucrites have positive ε^{142}Nd values in agreement with their high Sm/Nd, resulting from igneous processes on their parent body. The error bars correspond to the internal precision ($2\sigma_{mean}$). Terrestrial samples (MORBs, kimberlites, and carbonatites of different ages and collected in diverse locations) measured using the same procedure (*27*) have been added to demonstrate the significant excess of 0.2 ε units in all the terrestrial material (samples and standard) relative to the mean chondritic value. All terrestrial samples were measured several times using the same procedures as were used for the chondrites. The uncertainties reported on the mean are 2σ.

Department of Terrestrial Magnetism, Carnegie Institution of Washington, 5241 Broad Branch Road, N.W., Washington, DC 20015, USA.

*To whom correspondence should be addressed. E-mail: boyet@dtm.ciw.edu

Chondritic $^{142}Nd/^{144}Nd$. Because of the small variations in $^{142}Nd/^{144}Nd$, ^{142}Nd studies generally use a terrestrial Nd standard to express the ^{142}Nd anomalies in samples by direct comparison between the two measurements $\{\varepsilon^{142}Nd = [(^{142}Nd/^{144}Nd)_{sample} / (^{142}Nd/^{144}Nd)_{standard} - 1] \times 10^4\}$ on the assumption that the terrestrial standard has chondritic $^{142}Nd/^{144}Nd$. This assumption was derived from measurements that showed no resolvable difference between the $^{142}Nd/^{144}Nd$ of chondrites and that of the laboratory standard. For example, works by Jacobsen and Wasserburg (*6*, *7*), which are the only published measurements of bulk chondrites that include $^{142}Nd/^{144}Nd$ data, reported an average $\varepsilon^{142}Nd$ of –0.04 ± 0.54 (2σ of the population) with a range from –0.5 ± 0.4 to +0.4 ± 0.4. Amelin and Rotenberg (*19*) reported measurements of individual chondrules and phosphates separated from a variety of chondrites that provide a ^{146}Sm-^{142}Nd isochron and would yield a present-day value of $\varepsilon^{142}Nd$ = 0.01 ± 0.83 for a $^{147}Sm/^{144}Nd$ of 0.1966. The relatively large errors reflect that these data were either obtained on an older generation of mass spectrometer; measured NdO^+ instead of Nd^+, thus requiring an additional correction for oxygen isotopic composition and further complicating correction for Ce, Pr, and Sm interference; or were run on small samples. Today, a precision of a few parts per million (ppm) on Nd isotope ratios can be obtained with the new generation of thermal ionization mass spectrometer (*2*, *20*).

We measured the isotopic composition of Sm and Nd on a Thermo-Finnigan Triton thermal ionization mass spectrometer using the Nd^+ ion beam on samples passed repeatedly through ion-exchange chemistry, in order to reduce Ce and Sm interferences to negligible levels. Details of the analytical procedures and all the raw isotopic data measured on these samples are provided in the supporting online material (*21*). All of the analyzed chondrites and basaltic eucrites have $^{142}Nd/^{144}Nd$ ratios lower than the La Jolla Nd standard by between –40 and –8 ppm (Table 1). The deviations compared with the terrestrial reference are clearly significant because the external precision (2σ) measured on repeated runs is lower than 7 ppm for both samples and standards (Fig. 1 and Table 1). Both the $^{142}Nd/^{144}Nd$ and $^{143}Nd/^{144}Nd$ ratios of the chondrites and basaltic eucrites are positively correlated with their $^{147}Sm/^{144}Nd$ ratios, but the very small spread in $^{147}Sm/^{144}Nd$ ratios does not allow for precise isochrons to be constructed (Fig. 2). The mean values of $^{147}Sm/^{144}Nd$, $^{143}Nd/^{144}Nd$, and $^{142}Nd/^{144}Nd$ for the chondrites we measured are 0.1948 ± 0.0018, 0.512611 ± 0.000048, and –0.20 ± 0.14 ε units, respectively ($^{142}Nd/^{144}Nd$ expressed relative to the average for La Jolla Nd). The data for the enstatite (E)-chondrite, Abee, were excluded from this average because of the relatively poor-quality data for this sample. The averages of the basaltic eucrites measured here are indistinguishable within error from these chondrite averages. The chondrite average Sm/Nd ratio is slightly lower than the average of previous chondrite determinations, but our data scatter along a 4.567-Ga ^{147}Sm-^{143}Nd isochron (Fig. 2A), overlapping other recent chondrite results (*8*). Increasing the measured Sm/Nd for the samples reported here by 0.2% to account for our low measured Sm/Nd for the California Institute of Technology n(Sm/Nd)β standard, compared with that reported by Patchett *et al*. (*8*), would increase the degree of overlap of these data. Earlier chondrite Sm-Nd results (*6*, *7*) are offset to slightly higher $^{147}Sm/^{144}Nd$ for a given $^{143}Nd/^{144}Nd$. This offset may be because these earlier results were measured as NdO^+ and a linear instead of exponential relationship was applied, normalizing to $^{150}Nd/^{142}Nd$ or $^{146}Nd/^{142}Nd$ for mass fractionation correction, all of which complicate data comparison at this level of precision.

Early terrestrial differentiation. The homogeneity of the $^{142}Nd/^{144}Nd$ ratio among terrestrial samples has been widely demonstrated, especially with studies on Archean samples, but also in MORBs, ocean island basalts, kimberlites, and carbonatites, where $^{142}Nd/^{144}Nd$ excesses of a few parts per million (5 to 30) have been measured only in 3.8-Ga samples from Isua (*1*, *2*, *22*–*28*). However, all of these $^{142}Nd/^{144}Nd$ values were always compared to the measured value for the terrestrial Nd standard. Thus, the difference between all measured terrestrial values and the $^{142}Nd/^{144}Nd$ ratio of chondrites was not evident. Our new chondrite data show that ^{142}Nd anomalies in terrestrial samples relative

Table 1. Sm-Nd isotope and concentration data for chondrite and eucrite samples. Sm and Nd concentrations were determined by isotope dilution on a spiked aliquot taken after dissolution. $^{143}Nd/^{144}Nd$ ratios are normalized to 0.511860 for the La Jolla Nd standard. $^{142}Nd/^{144}Nd$ ratios are expressed in epsilon notation relative to La Jolla Nd (*21*). For Nuevo Laredo, Pasamonte, and one Sharp, Nd isotopic measurements were made on the same aliquot (only one dissolution) but loaded on separate filaments run in different barrels. The analytical uncertainties correspond to internal within-run precision (2σm). The external reproducibility on the $^{142}Nd/^{144}Nd$ ratio is about 7 ppm, except for Pasamonte. The lower precision reported for one measurement of Sharp and for Abee is explained by the small Nd signal. Dissolution in steel-jacket Teflon bombs or closed beakers on a hot plate produced no difference in results. The $\varepsilon^{149}Sm$ of 0 [$^{149}Sm/^{152}Sm$ ratios relative to the mean of the Sm standard (n = 7 samples)] measured for different samples signifies that isotopic ratios have not been significantly affected by neutron fluence effects. The internal precision on $\varepsilon^{149}Sm$ is lower than 0.3 ε units. Bas. Euc., basaltic eucrite; Cum. Euc., cumulate eucrite.

Meteorite name	Class	Sm	Nd	$^{147}Sm/^{144}Nd$	$^{143}Nd/^{144}Nd$ ± 2σm	$\varepsilon^{142}Nd$ ± 2σm	$\varepsilon^{149}Sm$
Allende*	CV3	0.3147	0.9858	0.1930	0.512573 ± 0.000003	–0.26 ± 0.07	–0.47
Allende	CV3	0.3238	1.010	0.1938	0.512563 ± 0.000002	–0.34 ± 0.05	–0.55
Allende	CV3	0.3128	0.9802	0.1929	0.512558 ± 0.000003	–0.31 ± 0.07	–0.64
Allende	CV3				0.512560 ± 0.000003	–0.32 ± 0.07	–0.25
Bruderheim	L6	0.1746	0.5399	0.1955	0.512620 ± 0.000003	–0.08 ± 0.08	0.19
Dhajala	H3.8	0.2012	0.6225	0.1954	0.512621 ± 0.000003	–0.19 ± 0.07	–0.58
Richardton*	H5	0.1912	0.5952	0.1942	0.512622 ± 0.000003	–0.16 ± 0.08	–2.17
Richardton	H5				0.512632 ± 0.000004	–0.20 ± 0.10	–2.60
Sharp	H3.4	0.1855	0.5722	0.1959	0.512624 ± 0.000006	–0.30 ± 0.15	–1.61
Sharp	H3.4	0.1901	0.5920	0.1951	0.512622 ± 0.000002	–0.16 ± 0.04	
					0.512627 ± 0.000003	–0.14 ± 0.06	
Abee	EH4	0.1460	0.4640	0.1903	0.512586 ± 0.000008	–0.40 ± 0.17	–0.20
Béréba	Bas. Euc.	1.699	5.284	0.1944	0.512597 ± 0.000002	–0.24 ± 0.05	0.09
Nuevo Laredo	Bas. Euc.	2.661	8.283	0.1942	0.512602 ± 0.000003	–0.19 ± 0.06	–0.34
					0.512601 ± 0.000002	–0.19 ± 0.05	
					0.512599 ± 0.000002	–0.21 ± 0.05	
Pasamonte	Bas. Euc.	2.293	7.126	0.1945	0.512598 ± 0.000002	–0.27 ± 0.05	–0.25
					0.512599 ± 0.000003	–0.15 ± 0.08	
Binda	Cum. Euc.	0.3566	0.9857	0.2187	0.513319 ± 0.000002	0.08 ± 0.05	0.60
Moama	Cum. Euc.	0.1575	0.3772	0.2523	0.514397 ± 0.000004	0.57 ± 0.09	–0.54
Moore County	Cum. Euc.	0.7071	2.082	0.2053	0.512996 ± 0.000003	0.05 ± 0.06	–0.36
					0.512988 ± 0.000007	0.10 ± 0.17	

*Dissolution in steel-jacket Teflon bomb.

to chondrites are not scarce; they are ubiquitous. Two explanations can account for this observation: (i) the BSE actually has an Sm/Nd ratio higher than that measured for chondrites, or (ii) all terrestrial rocks derive from a mantle reservoir with a high Sm/Nd ratio formed during the short lifetime of ^{146}Sm, that is, in the first 300 My of solar-system history. Given the refractory lithophile nature of both Sm and Nd and the small range of Sm/Nd ratios measured in different types of chondrites, there is no obvious reason to expect the BSE to have a higher-than-chondritic Sm/Nd ratio, but this option is not impossible. Regardless of whether the high ^{142}Nd/^{144}Nd ratios of terrestrial rocks reflect a nonchondritic Sm/Nd ratio in the BSE or an early differentiation event, the result requires major revision of models of the evolution and structure of Earth's interior.

The evolution of the 20-ppm excess in the ^{142}Nd/^{144}Nd ratios observed in terrestrial rocks requires a superchondritic Sm/Nd ratio, the magnitude of which depends on when the high Sm/Nd ratio was formed. The later the high Sm/Nd reservoir formed, the higher its Sm/Nd ratio must be to evolve the observed excess in ^{142}Nd/^{144}Nd value compared with that of chondrites. Because the Sm/Nd ratio also affects evolution of the ^{143}Nd/^{144}Nd value, any formation time for this reservoir more than 30 My after solar system formation would require an Sm/Nd ratio so high that the reservoir would evolve a ^{143}Nd/^{144}Nd value higher than that measured in MORBs (Fig. 3). For formation times of 4.562 and 4.537 Ga, the ^{147}Sm/^{144}Nd ratios needed to evolve a 20-ppm excess in ^{142}Nd/^{144}Nd value over the average chondrite value in our data are 0.209 and 0.212, respectively, which translate into present-day ^{143}Nd/^{144}Nd ratios of 0.513041 (ε^{143}Nd = +8.4) and 0.513129 (ε^{143}Nd = +10.1). These values overlap the range of Nd isotopic compositions measured in MORBs and also pass through the data for Archean samples (Fig. 4A).

Size and composition of early terrestrial reservoirs. Because all terrestrial rocks analyzed so far have ^{142}Nd/^{144}Nd values higher than our chondritic values, including the Isua samples, which are higher still, the early-formed high Sm/Nd reservoir inside Earth must have been the primary source for crust formation throughout at least the last 4 Gy of Earth's history. Constraints on the size and composition of the high Sm/Nd reservoir (termed here the "early depleted reservoir" or EDR), and its low Sm/Nd complement (termed the "early enriched reservoir" or EER) can be derived by considering the effect that the continental crust extraction would have on the composition of the mantle from which it was derived. Models relating depletion of the MORB mantle to extraction of the continental crust (*9–11*) use the mass balance equation of elements between continental crust and depleted mantle

$$[x]_{CC} \times M_{CC} + [x]_{MORBs} \times M_{MORBs} = [x]_{BSE} \times M_{BSE} \quad (1)$$

where $[x]$ represents the concentration of element x in the continental crust (CC), MORB source mantle (MORBs), and BSE, and M is the mass of these reservoirs. Given estimates for the average composition of continental crust (*29*), the depleted mantle (*30*), the BSE (*31*), and the known mass of the continental crust, this equation can be solved, providing the one-third to one-half value mentioned earlier (*9–11*). However, the nonchondritic ^{142}Nd/^{144}Nd of all terrestrial rocks requires a new mass balance equation

$$[x]_{CC} \times M_{CC} + [x]_{MORBs} \times M_{MORBs} = [x]_{EDR} \times M_{EDR} \quad (2)$$

The Sm/Nd ratio needed to evolve the superchondritic terrestrial ^{142}Nd/^{144}Nd results in a present-day ^{143}Nd/^{144}Nd value close to the value measured for the MORB. Therefore, the extraction of continental crust from this already-depleted reservoir (the EDR) cannot have greatly increased the Sm/Nd ratio of the MORB source; otherwise its ^{143}Nd/^{144}Nd value would have evolved to higher values than those observed for any terrestrial rock.

In order to minimize the effect of continent extraction on the degree of compositional fractionation of the residual mantle, the volume of mantle from which the continental crust was extracted must be large. For example, if the EDR was formed at 4.53 Ga, the ^{147}Sm/^{144}Nd ratio of 0.213 that is needed to evolve the terrestrial ^{142}Nd/^{144}Nd value is well matched by adding continental crust (*29*) to mantle with MORB source composition (*30*), only if the volume of mantle is as large as the whole mantle overlying the D″ layer. In other words, roughly 96% of the mantle must be as incompatible element–depleted as the MORB source, if the continents formed from an EDR with an Sm/Nd ratio high enough to explain the terrestrial ^{142}Nd/^{144}Nd value. Sufficient uncertainty exists in the crustal and MORB source compositions to allow a slightly smaller EDR, but the overriding result is that mantle that is compositionally similar to the MORB source must occupy most of the mantle.

The nonchondritic ^{142}Nd/^{144}Nd value of terrestrial rocks diminishes the importance of a chondritic, or BSE, composition source in the interpretation of the chemical and isotope systematics of Earth. The observation that the Nd-Hf isotope correlation displayed by oceanic basalts does not simultaneously pass through chondritic Hf and Nd isotopic composition is a problem that has led to debate (*32*). But there is no reason why this correlation should pass through chondritic composition if these reservoirs were derived from an EDR instead of the BSE. Similarly, the correlation between Nd and Sr isotopic composition defined by oceanic basalts has been used to estimate the BSE values of Sr isotopic composition, and hence Rb/Sr ratio, on the as-

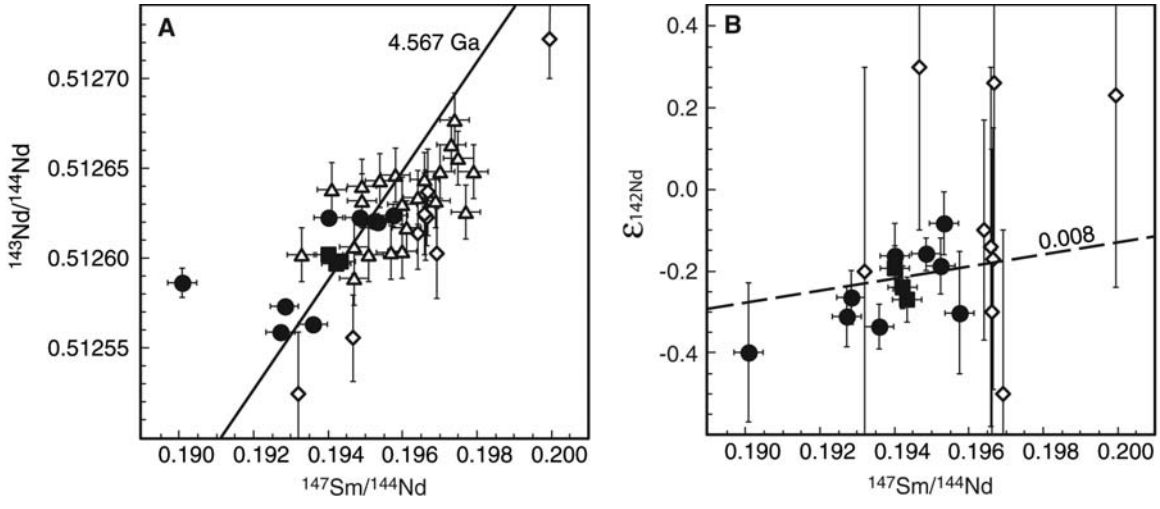

Fig. 2. (**A**) ^{147}Sm-^{143}Nd isochron diagram for chondrites (solid circles) and basaltic eucrites (solid squares) measured in this work. Our data and all previous chondrite measurements (open symbols) scatter along a 4.567-Ga isochron (*44*). Diamonds are from (*6*, *7*) and triangles are from (*8*). Errors bars correspond to the internal precision (2σ). (**B**) ^{146}Sm-^{142}Nd evolution diagram plots as ε^{142}Nd versus ^{147}Sm/^{144}Nd. The symbols are the same as in (A). Shown for reference is a line corresponding to ^{142}Nd/^{144}Nd evolution with the estimated solar system initial ^{146}Sm/^{144}Nd of ~0.008 (*45–48*).

sumption that Earth should have a chondritic Sm/Nd ratio. This assumption is no longer valid, at least for the portion of the mantle that has participated in crust formation. Thus, the BSE concentration of elements such as Rb and Pb, whose volatility and/or siderophile (metallic phase) nature make it unlikely that they are present in chondritic relative abundances in the BSE, depends strongly on the composition of the complementary enriched reservoir produced during early terrestrial differentiation.

A missing reservoir? The lack of terrestrial samples with subchondritic $^{142}Nd/^{144}Nd$ values indicates either that the BSE has a superchondritic Sm/Nd ratio or that the EER that is complementary to the early-formed EDR has never substantially participated in surface volcanism; thus, its composition is poorly constrained. An estimate of the composition of the EER can be obtained from a similar mass-balance approach on the assumption that EDR + EER = BSE, approximating the EDR composition by using that estimated for the MORB source mantle (*30*). This approach depends on the accuracy of the BSE composition, which, for the reasons described above, is now robust only for refractory lithophile elements, and on whether the MORB source is an adequate representation of the composition of the EDR. As shown in Fig. 5, if the EER is small, for example, the size of the D″ layer, then it must be quite enriched in incompatible elements to explain the magnitude of incompatible element depletion in the EDR. If the EER is as large as the mantle beneath 1600 km (*14*), then it will be considerably less enriched than a D″ EER, but still enriched by about a factor of 2 in most incompatible elements as compared with the BSE. The EER, regardless of its size, would thus contain about 43% of Earth's U, Th, and K, leading to ~9 TW of heat production. The lack of a signature of any low $^{142}Nd/^{144}Nd$ reservoir in crustal rocks suggests that the EER could reside at the base of the mantle and has not participated in producing rocks sampled at Earth's surface. As such, there is no compelling reason to assume that mantle convection is layered at mid-mantle depths based on the Sm-Nd data, but that there is a convective boundary at great depth in the mantle that has effectively isolated the small EER part of the mantle, unless the BSE has a nonchondritic composition. A similar model for a deep enriched reservoir and its implications for high heat production and for the rare gas evolution of Earth has recently been presented (*18*). In these models, the EER could serve both as a heat source for plume formation (*33*) and as a warm blanket to keep the outer core molten throughout Earth history and provide the energy needed to drive the geodynamo (*34*).

How the EER formed is suggested by the smooth BSE-normalized incompatible-element patterns calculated here for the EER. Most of the elements shown in Fig. 5 are refractory

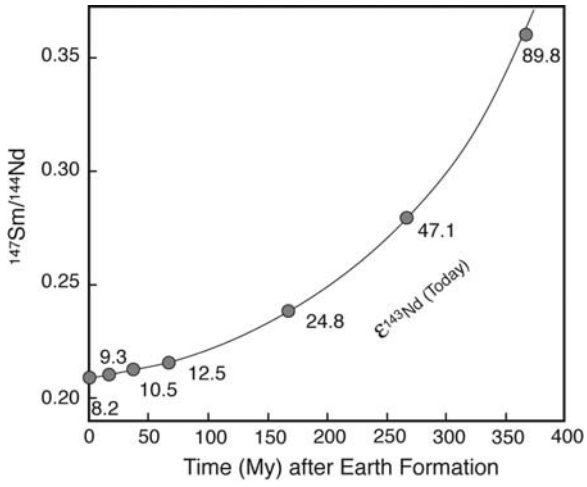

Fig. 3. Sm/Nd ratios needed to produce a 20-ppm excess in $^{142}Nd/^{144}Nd$ ratios, depending on when the Sm/Nd ratio is increased from the average chondritic value. The later the fractionation event, the higher the Sm/Nd ratio must be in the second stage to evolve the observed terrestrial excess in $^{142}Nd/^{144}Nd$ as compared to chondrites. The corresponding present-day $^{143}Nd/^{144}Nd$ ratios [expressed as $\varepsilon^{143}Nd$ relative to the average chondrite values of (*6*)] for these Sm/Nd ratios are shown for a few points along the curve. High Sm/Nd reservoirs formed during the first 30 My of Earth's history would be characterized today by an $\varepsilon^{143}Nd$ value lower than +10 ($^{147}Sm/^{144}Nd \sim 0.21$).

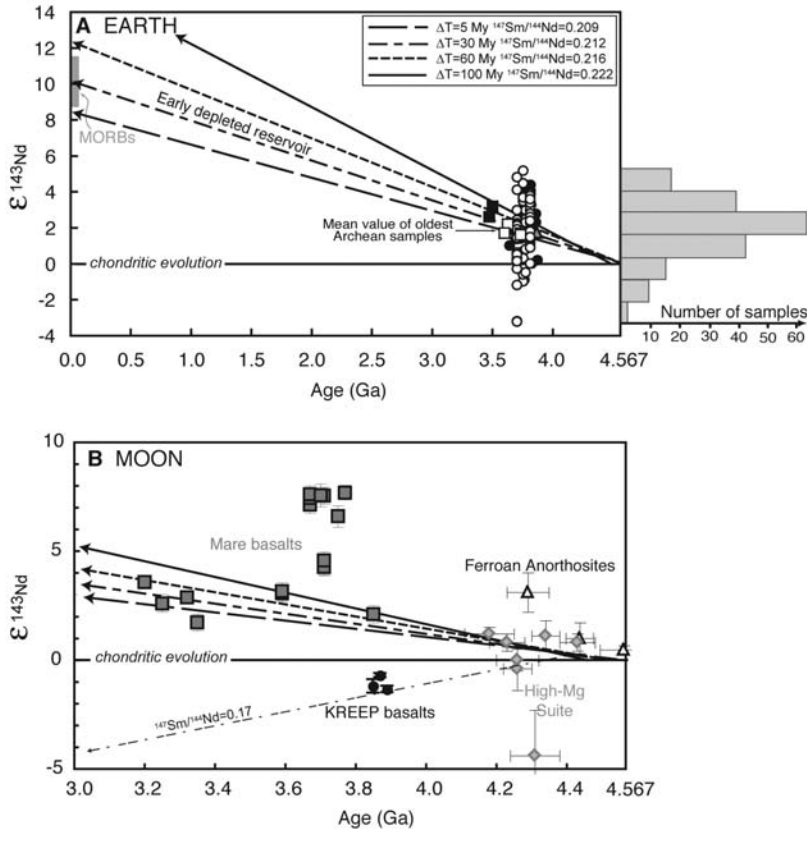

Fig. 4. (**A**) $\varepsilon^{143}Nd$ evolution of the early depleted reservoir on Earth as a function of the time of its formation. The different evolution lines were calculated considering an excess of 20 ppm for the $^{142}Nd/^{144}Nd$ ratio in Earth's mantle relative to chondrites. Each evolution line is defined by a specific slope dependent on the magnitude of the Sm/Nd fractionation and the age of the differentiation event (ΔT). A solar system initial $^{146}Sm/^{144}Sm$ of 0.008 (*45*, *46*) at 4.567 Gy (*44*) was used for these calculations, and we consider the mean values determined in this study for the chondritic reservoir. The geochemical data [i.e., the radiogenic $^{143}Nd/^{144}Nd$ ratios measured in most of the Archean samples (*49*–*53*)] (mean of +2 $\varepsilon^{143}Nd$), and the range of MORB values (+9 to +12), are best fit if the differentiation event occurred during the first 30 My of Earth's history. (**B**) Nd isotopic evolution for lunar samples [see (*54*) for recent review]. The superchondritic $^{142}Nd/^{144}Nd$ of the lunar samples (*12*) and the similarity to terrestrial values suggest that the Moon formed by a giant impact with Earth after Earth had undergone global differentiation. A superchondritic Sm/Nd in the bulk Moon is in agreement with the radiogenic $\varepsilon^{143}Nd$ reported for the oldest lunar samples (High-Mg suite samples and ferroan anorthosites). The lunar $^{142}Nd/^{144}Nd$ evolution is complicated by a second stage, the crystallization of the lunar magma ocean. The age of the second fractionation corresponds to the intersection of the lunar mantle evolution with the KREEP line ($^{147}Sm/^{144}Nd = 0.17$) at 4.42 Gy, implying that the lunar magma ocean required about 120 My to crystallize. Error bars are 2σ.

lithophile elements, and this observation is unlikely to be affected by revisions in BSE concentrations, except for elements such as Rb and Pb. The order of elements on the *x* axis is based on the relative incompatibility of these elements during shallow melting of the mantle (*11*), and thus depends primarily on the partition coefficients of clinopyroxene, a phase stable only in the upper few hundred kilometers of the mantle. The smooth patterns for the EER thus suggest that this reservoir was not formed by fractionation of some high-pressure phase such as perovskite, particularly given the distribution coefficients of trace elements recently measured for both Ca- and Mg-perovskite (*35*). Instead, a better analog for the EER may be the KREEP (basalts rich in K, rare earth elements, and P) component of the Moon, which is a highly incompatible element–enriched residual liquid believed to have formed at low pressure by near-complete crystallization of a lunar magma ocean (*36*). If the terrestrial EER also formed at shallow depth, its lack of contribution to surface volcanism suggests that it now must reside in the deep mantle. The sinking of a dense, Fe- and Ti-rich residual liquid like KREEP through the lunar mantle has been modeled (*37*). A similar event may have happened to a shallow terrestrial EER, taking it from near Earth's surface to the base of the mantle. Such a dense layer could be stable at great depth and remain poorly mixed with the rest of the mantle over the age of Earth (*33*). The small deficit in ^{142}Nd (–10 ppm relative to the terrestrial standards) recently reported in a few flood basalts from the Deccan Province (*38*) could indicate some mixing of the enriched deep material with depleted overlying mantle.

Implications for Mars and Earth's Moon. The new chondritic ^{142}Nd/^{144}Nd value also requires a revision of the interpretation of the early evolution of other planetary bodies, in particular the Moon and Mars. Martian rocks (as sampled by the SNC meteorites) span a wide range of ^{142}Nd/^{144}Nd values [from +90 ppm to –20 ppm, relative to the terrestrial standard (*4*)]. Compared with the terrestrial ^{142}Nd/^{144}Nd values, martian ^{146}Sm-^{142}Nd systematics allow the differentiation of the silicate portion of Mars to have occurred as late as 40 My after solar system formation (*5*). Using instead the new chondritic value for the ^{142}Nd/^{144}Nd ratio requires that this time interval be shortened. Martian core formation dated with ^{182}Hf-^{182}W and mantle differentiation could have occurred simultaneously at ~12 My after solar system formation (*5*, *39*).

Most lunar samples have ^{142}Nd/^{144}Nd values close to terrestrial values, with the exception of some high-Ti basalts, which have values that are 20 ppm higher (*3*). The new chondrite values mean that all lunar samples, like Earth's, have superchondritic ^{142}Nd/^{144}Nd ratios. This suggests that the Moon formed from a giant impact into an already-differentiated Earth, sampling the depleted reservoir that also has been the source of terrestrial crustal rocks. Numerical simulations of a giant impact origin for the Moon suggest that at least two-thirds of the material that makes up the Moon is derived from the impactor, not from Earth (*40*). This expectation is difficult to reconcile with the similar nonchondritic lunar and terrestrial ^{142}Nd/^{144}Nd ratios, unless the impactor had a similar history of silicate differentiation as did the early Earth. Nevertheless, the superchondritic lunar ^{142}Nd/^{144}Nd value is consistent with the superchondritic initial ^{143}Nd/^{144}Nd value measured for the oldest lunar crustal samples (Fig. 4B) (*41*–*43*).

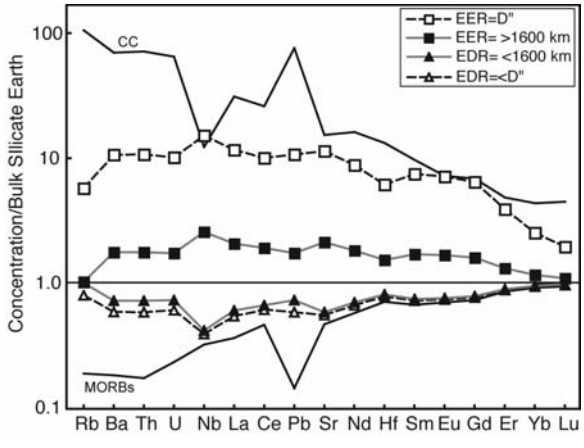

Fig. 5. BSE (*31*) normalized trace element abundances for early-differentiated reservoirs of different sizes. These curves are calculated by assuming that the ^{147}Sm/^{144}Nd of the EDR is 0.21, needed to evolve the 20-ppm terrestrial excess in ^{142}Nd/^{144}Nd for a reservoir formation age of 30 My after Earth formation. The remaining elemental compositions of the EDR are then calculated by adding average continental crust (*29*) to average MORB source mantle (*30*) until this Sm/Nd is achieved. The composition of the EER is then calculated on the assumption that the composition of the EER and EDR sum to BSE (*31*) for the various assumed mass ratios of EER and EDR shown in the figure.

References and Notes

1. M. Boyet *et al.*, *Earth Planet. Sci. Lett.* **214**, 427 (2003).
2. G. Caro, B. Bourdon, J.-L. Birck, S. Moorbath, *Nature* **423**, 428 (2003).
3. L. E. Nyquist *et al.*, *Geochim. Cosmochim. Acta* **59**, 2817 (1995).
4. C. L. Harper Jr., L. E. Nyquist, B. Bansal, H. Wiesmann, C.-Y. Shih, *Science* **267**, 213 (1995).
5. C. N. Foley *et al.*, *Geochim. Cosmochim. Acta*, in press.
6. S. B. Jacobsen, G. J. Wasserburg, *Earth Planet. Sci. Lett.* **50**, 139 (1980).
7. S. B. Jacobsen, G. J. Wasserburg, *Earth Planet. Sci. Lett.* **67**, 137 (1984).
8. P. J. Patchett, J. D. Vervoort, U. Söderlund, *Earth Planet. Sci. Lett.* **222**, 29 (2004).
9. S. B. Jacobsen, G. J. Wasserburg, *J. Geophys. Res.* **84**, 7411 (1979).
10. C. J. Allègre, S. R. Hart, J.-F. Minster, *Earth Planet. Sci. Lett.* **66**, 191 (1983).
11. A. W. Hofmann, *Earth Planet. Sci. Lett.* **90**, 297 (1988).
12. F. Albarède, R. D. Van der Hilst, *Philos. Trans. R. Soc. London Ser. A* **360**, 2569 (2002).
13. P. E. van Keken, E. H. Hauri, C. J. Ballentine, *Annu. Rev. Earth Planet. Sci.* **30**, 493 (2002).
14. L. H. Kellogg, B. H. Hager, R. D. Van der Hilst, *Science* **283**, 1881 (1999).
15. V. C. Bennett, in *Treatise on Geochemistry, Volume 2—The Mantle and Core*, H. D. Holland, K. K. Turekian, R. W. Carlson, Eds. (Elsevier, Oxford, 2003), pp. 493–520.
16. S. A. Wilde, J. W. Valley, W. H. Peck, C. M. Graham, *Nature* **409**, 175 (2001).
17. C. J. Allègre, T. Staudacher, P. Sarda, M. Kurz, *Nature* **303**, 762 (1983).
18. I. Tolstikhin, A. W. Hofmann, *Phys. Earth Planet. Int.* **148**, 109 (2005).
19. Y. Amelin, E. Rotenberg, *Earth Planet. Sci. Lett.* **223**, 267 (2004).
20. M. Sharma, C. Chen, *Precamb. Res.* **135**, 315 (2004).
21. Materials and methods are available as supporting material on *Science* Online.
22. V. C. Bennett, M. T. McCulloch, *Trans. Am. Geophys. Union* **73**, 621 (1992).
23. S. J. G. Galer, S. L. Goldstein, *Trans. Am. Geophys. Union* **73**, 622 (1992).
24. C. L. Harper, S. B. Jacobsen, *Nature* **360**, 728 (1992).
25. M. Regelous, K. D. Collerson, *Geochim. Cosmochim. Acta* **60**, 3513 (1996).
26. M. Sharma, D. A. Papanastassiou, G. J. Wasserburg, R. F. Dymek, *Geochim. Cosmochim. Acta* **60**, 2037 (1996).
27. M. Boyet, R. W. Carlson, *EoS* **85**, abstract U41A-0723 (2004).
28. M. Boyet, M. O. Garcia, R. Pik, F. Albarède, *Geophys. Res. Lett.* **32**, L04306 (2005).
29. R. L. Rudnick, S. Gao, in *Treatise on Geochemistry, Volume 3—The Crust*, H. D. Holland, K. K. Turekian, Eds. (Elsevier-Pergamon, Oxford, 2003), pp. 1–64.
30. V. J. M. Salters, A. Stracke, *Geochem. Geophys. Geosyst.* **5**, 10.1029/2003GC000597 (2004).
31. W. F. McDonough, S.-s. Sun, *Chem. Geol.* **120**, 223 (1995).
32. J. Blichert-Toft, F. Albarède, *Earth Planet. Sci. Lett.* **148**, 243 (1997).
33. H. Samuel, C. G. Farnetani, *Earth Planet. Sci. Lett.* **207**, 39 (2003).
34. B. A. Buffett, *Science* **299**, 1675 (2003).
35. A. Corgne, C. Liebske, B. J. Wood, D. C. Rubie, D. J. Frost, *Geochim. Cosmochim. Acta* **69**, 485 (2005).
36. P. H. Warren, J. T. Wasson, *Rev. Geophys. Space Phys.* **17**, 73 (1979).
37. E. M. Parmentier, S. Zhong, M. T. Zuber, *Earth Planet. Sci. Lett.* **201**, 473 (2002).
38. R. Andreasen, K. V. Subbarao, M. Sharma, *Geochim. Cosmochim. Acta* **68**, A747 (2004).
39. T. Kleine, C. Münker, K. Mezger, H. Palme, *Nature* **418**, 952 (2002).
40. R. M. Canup, *Icarus* **168**, 433 (2004).
41. R. W. Carlson, G. W. Lugmair, *Earth Planet. Sci. Lett.* **90**, 119 (1988).
42. C. Alibert, M. D. Norman, M. T. McCulloch, *Geochim. Cosmochim. Acta* **58**, 2921 (1994).
43. L. E. Borg *et al.*, *Geochim. Cosmochim. Acta* **63**, 2679 (1999).
44. Y. Amelin, A. N. Krot, I. D. Hutcheon, A. A. Ulyanov, *Science* **297**, 1678 (2002).
45. G. W. Lugmair, J. G. Galer, *Geochim. Cosmochim. Acta* **56**, 1673 (1992).
46. A. Prinzhofer, D. A. Papanastassiou, G. J. Wasserburg, *Geochim. Cosmochim. Acta* **56**, 797 (1992).
47. L. E. Nyquist, B. Bansal, H. Wiesmann, C.-Y. Shih, *Meteoritics* **29**, 872 (1994).
48. B. W. Stewart, D. A. Papanastassiou, G. J. Wasserburg, *Geochim. Cosmochim. Acta* **58**, 3487 (1994).
49. B. M. Jahn *et al.*, *Precamb. Res.* **34**, 311 (1987).
50. S. B. Jacobsen, R. F. Dymek, *J. Geophys. Res.* **93**, 338 (1988).
51. G. Gruau, M. Rosing, D. Bridgwater, R. C. O. Gill, *Chem. Geol.* **133**, 225 (1996).
52. V. C. Bennett, A. P. Nutman, M. T. McCulloch, *Earth Planet. Sci. Lett.* **119**, 299 (1993).
53. J. D. Vervoort, J. Blichert-Toft, *Geochim. Cosmochim. Acta* **63**, 533 (1999).

54. G. A. Snyder, L. E. Borg, L. E. Nyquist, L. A. Taylor, in *Origin of the Earth and Moon*, R. M. Canup, K. Righter, Eds. (Univ. of Arizona Press, Tucson, AZ, 2000), pp. 361–395.

55. Acquisition of our Triton mass spectrometer was made possible by NSF grant EAR-0320589 and a matching contribution from the Carnegie Institution of Washington. We thank G. Tilton for generously donating his meteorite collection to D.T.M., which facilitated this project. Abee and Allende are from the Smithsonian (United States National Museum nos. 6581 and 3329, respectively), provided by T. McCoy. We thank M. Horan and T. Mock for analytical support and S. Shirey and two anonymous reviewers for their constructive comments that greatly benefited the paper.

Supporting Online Material
www.sciencemag.org/cgi/content/full/1113634/DC1
Materials and Methods
Fig. S1
Table S1
References

15 April 2005; accepted 8 June 2005
Published online 16 June 2005;
10.1126/science.1113634
Include this information when citing this paper.

Crystal Structure of Human Toll-Like Receptor 3 (TLR3) Ectodomain

Jungwoo Choe, Matthew S. Kelker, Ian A. Wilson*

Toll-like receptors (TLRs) play key roles in activating immune responses during infection. The human TLR3 ectodomain structure at 2.1 angstroms reveals a large horseshoe-shaped solenoid assembled from 23 leucine-rich repeats (LRRs). Asparagines conserved in the 24-residue LRR motif contribute extensive hydrogen-bonding networks for solenoid stabilization. TLR3 is largely masked by carbohydrate, but one face is glycosylation-free, which suggests its potential role in ligand binding and oligomerization. Highly conserved surface residues and a TLR3-specific LRR insertion form a homodimer interface in the crystal, whereas two patches of positively charged residues and a second insertion would provide an appropriate binding site for double-stranded RNA.

Innate immunity is based on an ancient and ubiquitous system of cells and molecules that defend the host against infection. This system can recognize virtually all microbes, using a limited repertoire of germ-line–encoded receptors that recognize broadly conserved components of bacterial and fungal cell walls or genetic material, such as double-stranded viral RNA (*1*, *2*).

The Toll-like receptors (TLRs) are among the most important sensors of the innate immune system (*3*). The ten known human Toll-like receptors recognize pathogen-associated molecules, such as lipoteichoic acid (recognized by TLR2), lipopolysaccharide (TLR4), flagellin (TLR5), and unmethylated CpG DNA motifs (TLR9). Binding of these ligands to TLRs initiates a series of signaling processes that stimulate and orchestrate the innate and adaptive immune responses (*4*, *5*). Human TLRs are implicated in a number of diseases and, hence, constitute potential therapeutic targets (*6*, *7*).

TLRs are integral membrane proteins located either on the cell surface or in intracellular compartments. Their extracellular or ectodomains (ECDs) are responsible for ligand binding and contain 19 to 25 leucine-rich repeat (LRR) motifs that are also found in a number of other proteins with diverse cellular functions (*8*). The intracellular domain, known as the Toll/interleukin-1 receptor homology (TIR) domain, recruits adaptor molecules, such as MyD88, TRIF, and TIRAP, to initiate the signaling process (*4*, *9*).

Human TLR3 is activated by double-stranded RNA (dsRNA) associated with viral infection (*10*), endogeneous cellular mRNA (*11*), and sequence-independent small interfering RNAs (*12*). TLR3 is distinct from other TLRs in that it is not dependent on MyD88 but rather on TRIF for signaling (*13*). Other key features of TLR3 signaling include a requirement for phosphorylation of tyrosine residues in the TIR domain (*14*) and the involvement of phosphatidylinositol-3 kinase (*15*). In turn, TLR3 activates genes for secreted antiviral cytokines, such as interferon (IFN-β), and those that encode intracellular, viral, stress-inducible proteins (*16*).

Overall structure. The complete ectodomain of human TLR3 without the N-terminal signal sequence (residues 27 to 700) was expressed using a baculovirus system and purified by Ni-nitrilotriacetic acid (NTA) affinity, ion-exchange, and size-exclusion chromatography

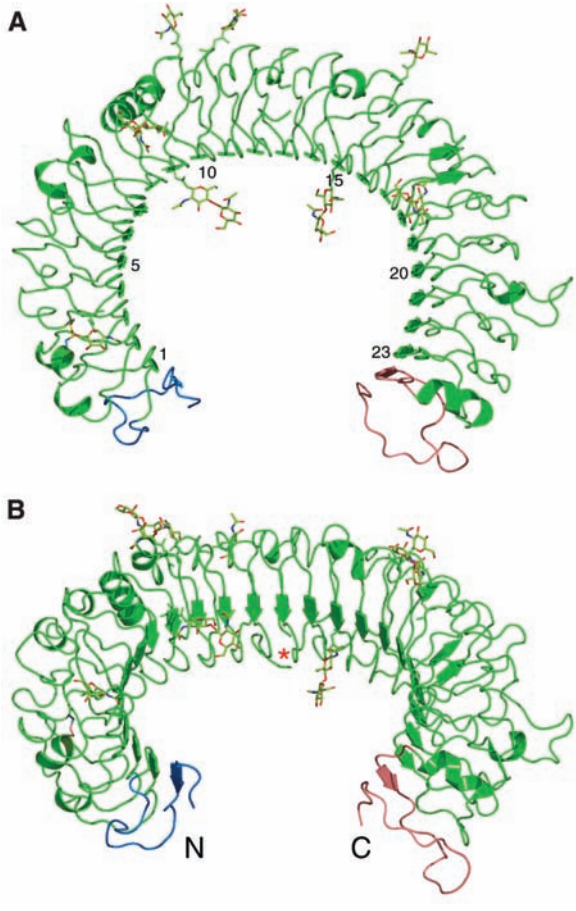

Fig. 1. Overall architecture of TLR3 ECD in a ribbon representation. The N-terminal cap region is colored blue; the 23 canonical LRRs are in green; and the C-terminal region is in pink. N-linked sugars (N-acetylglucosamines) that are observed in the electron density maps are shown in ball-and-stick representation, attached to their respective Asn residues. The disulfide bond linking LRRs 2 and 3 is drawn in orange, adjacent to the glycosylation site. **(A)** Side view of TLR3 with the convex face pointing outwards, the concave face inwards, and the heavily glycosylated side face pointing toward the viewer. **(B)** View rotated 45° from (A) that highlights the continuous β sheet that forms the concave surface. The position of the large insertion in LRR12 that extends toward the glycosylation-free face is marked with an asterisk.

Department of Molecular Biology and The Skaggs Institute for Chemical Biology, The Scripps Research Institute (TSRI), 10550 North Torrey Pines Road, La Jolla, CA 92037, USA.

*To whom correspondence should be addressed. E-mail: wilson@scripps.edu